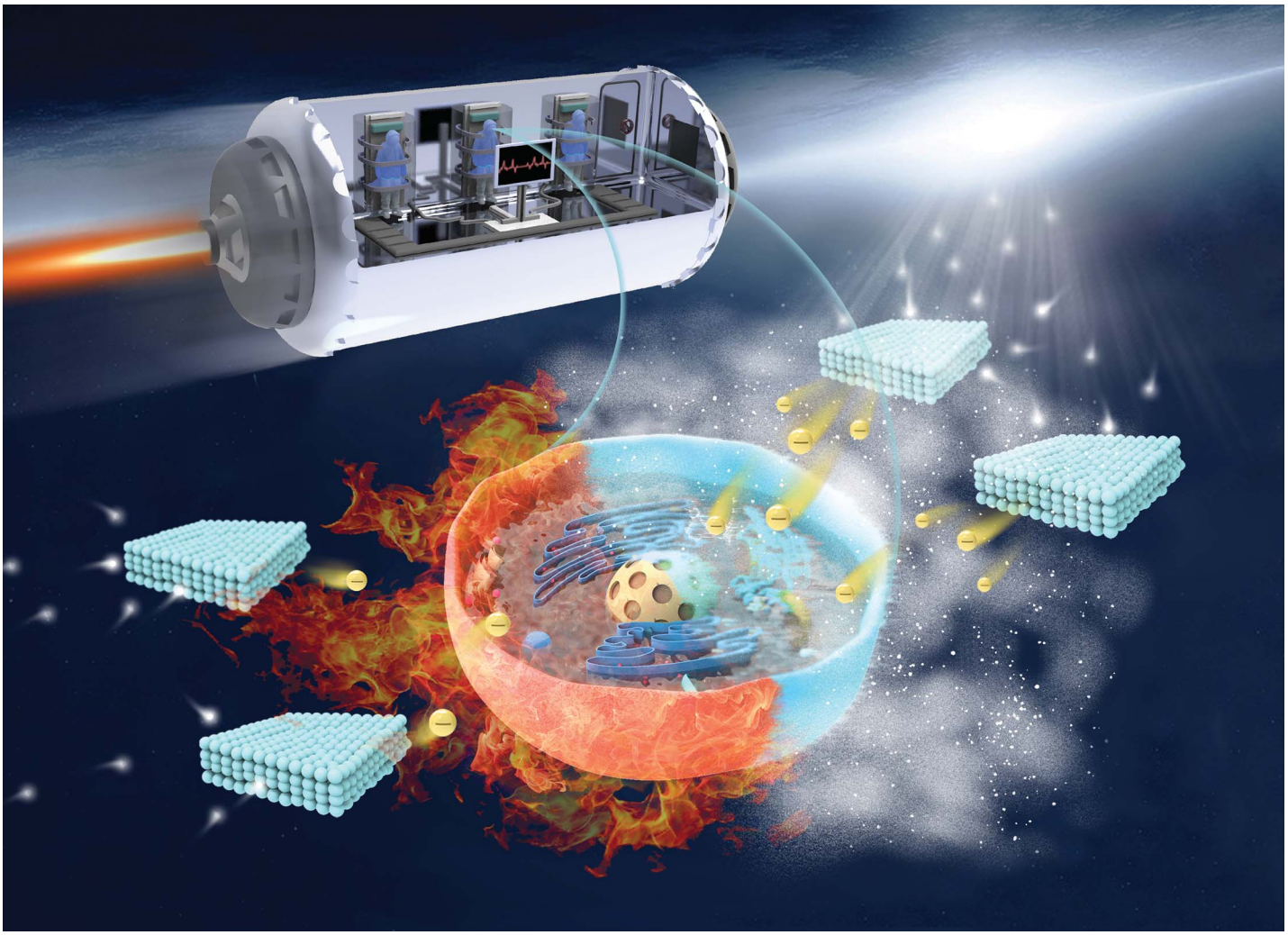

Showcasing research from Professor Aiguo Wu's laboratory, Cixi Institute of Biomedical Engineering, Ningbo Institute of Materials Technology and Engineering, Chinese Academy of Science, Ningbo, China.

Low temperature-boosted high efficiency photo-induced charge transfer for remarkable SERS activity of ZnO nanosheets

The decreased traps of photo-induced electrons at surface defect states effectively facilitate the PICT efficiency within the substrate–molecule system. This study not only provides a deep insight into the chemical SERS mechanism, but also develops a novel strategy for improving semiconductor SERS sensitivity. The strong SERS activity at a low temperature reported here may open new avenues for developing non-metal SERS substrates with new functionalities, especially for research on cryogenic sensing and hypothermal medicine.

As featured in:

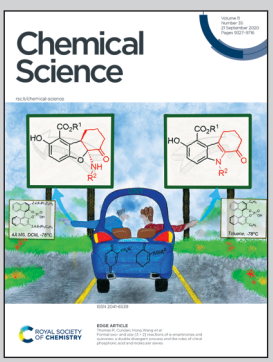

See Xiaotian Wang, Tianxiang Chen, Lin Guo, Aiguo Wu *et al.*, *Chem. Sci.*, 2020, **11**, 9414.

ROYAL SOCIETY OF CHEMISTRY

rsc.li/chemical-science

Registered charity number: 207890

Chemical Science

ROYAL SOCIETY OF CHEMISTRY

EDGE ARTICLE

Cite this: *Chem. Sci.*, 2020, **11**, 9414

All publication charges for this article have been paid for by the Royal Society of Chemistry

Low temperature-boosted high efficiency photo-induced charge transfer for remarkable SERS activity of ZnO nanosheets†

Jie Lin,‡[a] Jian Yu,‡[b] Ozioma Udochukwu Akakuru,[a] Xiaotian Wang,[*b] Bo Yuan,[a] Tianxiang Chen,[*a] Lin Guo[*b] and Aiguo Wu[*a]

Improving the photo-induced charge transfer (PICT) efficiency is the key factor for boosting the surface-enhanced Raman scattering (SERS) performance of semiconductor nanomaterials. Introducing plentiful surface defect states in porous ZnO nanosheets (d-ZnO NSs) effectively provides additional charge transfer routes for highly efficient PICT within the substrate–molecule system. Significantly, an interesting phenomenon of low temperature-boosted SERS activity of these d-ZnO NSs is consequently observed. The enhanced SERS activity can be attributed to the efficient PICT processes due to the significant reduction of non-radiative recombination of surface defects at a low temperature. This is carefully investigated through combining *in situ* low-temperature SERS measurements with temperature-dependent photoluminescence (PL) emission spectroscopy. Our results clearly demonstrate that the weakened lattice thermal vibration at a low temperature effectively suppresses the phonon-assisted relaxation and reduces carrier traps, resulting in the increase of PL intensity. The decreased traps of photo-induced electrons at surface defect states effectively facilitate the PICT efficiency within the substrate–molecule system. An ultrahigh enhancement factor of 7.7×10^5 and low limit of detection (1×10^{-7} M) for a 4-mercaptopyridine molecule at a temperature of 77 K are successfully obtained. More importantly, the low temperature-enhanced SERS effect is also obtainable in other metal oxide semiconductors, such as d-TiO_2 and d-Cu_2O nanoparticles. To the best of our knowledge, this is the first time the low temperature-boosted SERS activity of semiconductors has been observed. This study not only provides a deep insight into the chemical SERS mechanism, but also develops a novel strategy for improving semiconductor SERS sensitivity. The strong SERS activity at a low temperature reported here may open new avenues for developing non-metal SERS substrates with new functionalities, especially for the research on cryogenic sensing and hypothermal medicine.

Received 12th May 2020
Accepted 13th August 2020

DOI: 10.1039/d0sc02712j

rsc.li/chemical-science

Introduction

Surface-enhanced Raman scattering (SERS) spectroscopy has attracted extensive attention in numerous research fields due to its fascinating advantages, including extremely high sensitivity, a non-destructive label-free detection mode, and molecular fingerprint features.[1–6] The SERS enhancement mechanism of noble metals (for example, Au, Ag, and Cu) primarily relies on the oscillations of free electrons in metals that could couple with the illuminated electromagnetic field, also called the surface plasmon resonance (SPR) mechanism.[7,8] The huge electromagnetic enhancement excited by the SPR mechanism could produce tremendous SERS enhancement factors (EFs) and greatly increase the SERS sensitivity, even fulfilling the requirement of single molecule detection.[9,10] For semiconductor materials, the charge transfer resonance efficiency is largely dependent on energy level overlap between the SERS substrate conduction/valence band and adsorbate HOMO/LUMO under incident light,[11] which plays a major role in SERS-active semiconductor substrates. Energy level overlap and vibrational coupling resonance in semiconductor–molecule SERS systems can effectively increase molecular polarizability and amplify Raman scattering cross-section of probe molecules.[12] The excitation wavelength of choice for semiconductor–molecule SERS systems is greatly dependent on the vibrational coupling modes of the photo-induced charge transfer process. For semiconductor-based substrates, the features of selective SERS enhancement,[13] high spectra reproducibility,[14] good

[a]*Cixi Institute of Biomedical Engineering, Chinese Academy of Science (CAS) Key Laboratory of Magnetic Materials and Devices, Zhejiang Engineering Research Center for Biomedical Materials, Ningbo Institute of Materials Technology and Engineering, CAS, 1219 Zhongguan West Road, Ningbo 315201, P. R. China. E-mail: aiguo@nimte.ac.cn; chentx@nimte.ac.cn*

[b]*School of Chemistry, Beihang University, Beijing 100191, P. R. China. E-mail: wangxt@buaa.edu.cn; guolin@buaa.edu.cn*

† Electronic supplementary information (ESI) available. See DOI: 10.1039/d0sc02712j

‡ J. Lin and J. Yu contributed equally.

biocompatibility,[15] and controllable surface modifiability,[16,17] endow semiconductor materials with unique advantages for a wide range of practical applications. However, relatively weak EF is a major obstacle for semiconductor SERS substrates to serve as ideal high-sensitivity chemical sensors. Many strategies have been proposed to effectively improve the PICT process, including three general chemical methods of element doping,[18] element extraction[19] and morphology design.[20] In these cases, the surface properties of the semiconductor materials are modulated to promote the photo-induced electron transition efficiency by increasing the electron concentration or providing additional transition pathways to facilitate the electron transition possibility. Introducing plentiful surface defects in semiconductor materials is also an effectual strategy to boost the SERS performance of semiconductor substrates.[21,22] Recently, amorphous semiconductor materials have been reported with significant PICT transitions in substrate–molecule systems benefitting from metastable electronic states.[23–25]

To improve the PICT efficiency within the substrate–molecule system, researcherse mainly focus on increasing the charge transfer pathways and vibronic coupling, while much less attention is channeled toward the non-radiative recombination of excitons, which will essentially deteriorate the PICT transitions. Thus, developing a facile strategy to overcome this vital issue is urgent. Low temperatures can effectively weaken the lattice thermal vibration and suppress phonon-assisted relaxation, thereby reducing the phonon-assisted non-radiative recombination.[26] In this regard, temperature-dependent phonon relaxation has been explored in previous studies. For instance, Lounis *et al.* indicated that $FAPbBr_3$ perovskite nanocrystals display an intense exciton emission due to the extremely reduced phonon-assisted radiation,[27] which was investigated *via* low-temperature photoluminescence (PL) spectroscopy. Herz *et al.* reported that charge-carrier mobility of $FASnI_3$ films is boosted about 7 times at an extremely low temperature, which is assisted by the reduced interactions with phonons.[28] Mahamuni *et al.* observed that $CsPbCl_3$ nanocrystals possess obviously enhanced defect-related electron emission by the low-temperature PL due to reduced carrier traps, resulting in an excitonic super-radiance effect.[29] These studies demonstrated that surface defect-related electron transfer in semiconductors can be effectively promoted at low temperatures. Therefore, using low temperature conditions may provide a promising strategy to facilitate the PICT process efficiency, and effectively improve the SERS activity of semiconductor substrates.

Inspired by the above-mentioned valuable discoveries, we successfully realized low temperature-boosted PICT transitions by effectively suppressing non-radiative recombination, which enabled an obviously enhanced SERS activity for semiconductors, such as ZnO, TiO_2 and Cu_2O nanomaterials. ZnO nanoparticles (NPs) have been proven to be one of the promising candidates among semiconductor SERS substrates, and here we take porous ZnO nanosheets (NSs) as an optimal platform to illustrate the low temperature-enhanced Raman scattering effect. Porous ZnO NSs enriched with abundant surface defect states (d-ZnO NSs) are successfully synthesized by a self-assembly strategy and demonstrate a remarkable SERS activity with an EF of 7.7×10^5 at a low temperature of 77 K. Surface defect states are in favor of introducing additional charge transfer routes to obtain highly efficient PICT resonances within the d-ZnO NS–molecule complex. Moreover, the low-temperature SERS condition provides an ideal environment to weaken lattice thermal vibration and reduce phonon-assisted relaxation, resulting in the increase of photo-induced electrons for highly efficient PICT transitions within the d-ZnO NS–molecule system. The increase of photo-induced electrons on defect energy levels is clearly observed from the low-temperature PL emission spectra. Furthermore, an obvious low temperature-boosted SERS activity is confirmed *via in situ* low temperature-SERS measurements of several probe molecules by using d-ZnO NSs. Significantly, this strategy of low-temperature SERS is also applicable to other semiconductor substrates, such as d-TiO_2 and d-Cu_2O NPs. To the best of our knowledge, this is the first evidence of using low-temperature conditions to effectively facilitate the interfacial PICT efficiency and obtain an ultrahigh SERS activity of semiconductors. We believe that the study presented herein will open a new frontier for optimizing and realizing high-sensitivity semiconductor substrates, which opens new avenues for the study of cryogenic sensing and hypothermal medicine.

Results and discussion

Based on the Herzberg–Teller coupling rule,[30,31] the effective charge transfer process contributing to the SERS effect is mainly dominated by the two electron transition modes: photo-induced electron transfer from molecular ground states ($|I\rangle$) to the semiconductor conduction band (CB) states ($|C\rangle$) *via* the transition moment μ_{IC}, and from the semiconductor valence band (VB) states ($|V\rangle$) to molecular excited states ($|K\rangle$) *via* the transition moment μ_{VK}. The feature of a large band gap severely limits several vibronic coupling modes in ZnO–molecule systems according to the thermodynamic rule in the PICT process.[32,33] Introducing surface defect states ($|S\rangle$) in ZnO NSs by a chemical synthesis strategy can effectively improve the PICT transition possibility *via* the additional transition moment, μ_{VS}, μ_{SK}, and μ_{IS} under laser illumination as illustrated in Fig. S1.† The numerous surface defect energy levels can serve as a springboard to assist the PICT transitions within the substrate–molecule system.

Photo-induced electrons participating in the PICT process are derived from the separation of excitons. However, exciton separation is partly suppressed by the phonon-assisted non-radiative recombination, which is caused by the lattice thermal vibration. Photo-induced electrons located at the defect states will easily undergo a phonon-assisted thermal recombination, which will deteriorate the PICT efficiency. A low-temperature environment can effectively reduce the lattice thermal vibration and decrease the phonon generation, thereby reducing the non-radiative recombination of excitons and increasing the number of photo-induced electrons to participate in the PICT transitions. Therefore, low-temperature SERS conditions might provide a promising strategy to suppress

phonons and promote electron transfer from surface-defect states to molecular excited states (transition moment: μ_{SK}) under laser illumination, as shown in Fig. 1. The facilitated photo-induced electron transfer pathways within the ZnO–molecule complex could significantly enhance the PICT transitions and help realize a remarkable SERS activity of d-ZnO nanostructures.

In order to confirm this hypothesis, we performed *in situ* low temperature-dependent SERS measurements by using d-ZnO nanomaterials as the platform, due to their strong SERS activity. The synthesis of porous d-ZnO NSs based on liquid phase synthesis routes follows our previous report with minor modifications,[34] and details of the synthesis process are given in the ESI.† Porous d-ZnO NSs exhibit a regular parallelogram morphology with obvious edges and corners. Typically, the size and thickness of porous d-ZnO NSs are ~300 and 20 nm, respectively, which are determined *via* the transmission electron microscopy (TEM) images shown in Fig. 2a and b. Porous d-ZnO NSs are generated by numerous randomly arranged ZnO NPs (~20 nm), which are employed as the building blocks in the self-assembly synthetic approach (Fig. S2†). Owing to the lattice fusion of neighboring ZnO NPs, abundant surface defect states are formed in the d-ZnO NSs shown in Fig. S3.† It can be clearly seen that the adjacent lattice fringes of d-ZnO NSs are 0.28 and 0.26 nm, which correspond to the lattice constants of the (100) and (002) planes of wurtzite-type hexagonal ZnO, respectively (Fig. 2c). In addition, the concentric rings assigned to the (100), (002), (101), (110), and (103) lattice planes can be easily discerned in the selected area of the electron diffraction (SAED) pattern (Fig. 2d), matching well with the X-ray diffraction (XRD) pattern (Fig. S4†), which verifies the wurtzite ZnO phase of these NSs (JSPDS 79-2205). The high-angle annular dark-field STEM (HAADF-STEM) image (Fig. 2e) and elemental maps (Fig. 2f and g) clearly demonstrate that the Zn and O atoms are distributed homogenously on the NSs.

The morphological advantage of the porous structure of d-ZnO NSs is beneficial to light harvesting and molecule adsorption due to the large surface area (96.5 m^2 g^{-1}) shown in Fig. S5a.† It is conceivable that the target molecules are adsorbed on the d-ZnO NS SERS substrate through chemical bonding

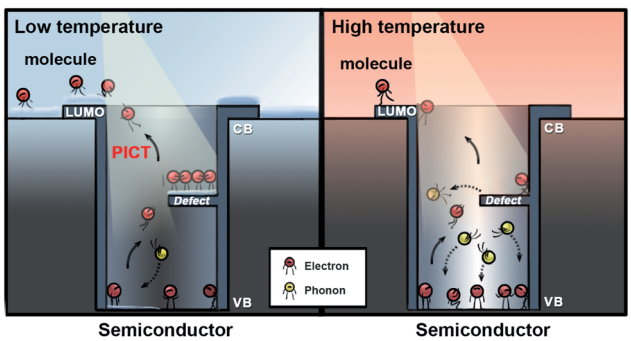

Fig. 1 The competitive relationship between the photo-induced electrons on surface defect states for PICT transitions and phonon-assisted non-radiative recombination in the semiconductor–molecule system at low and high temperatures, respectively.

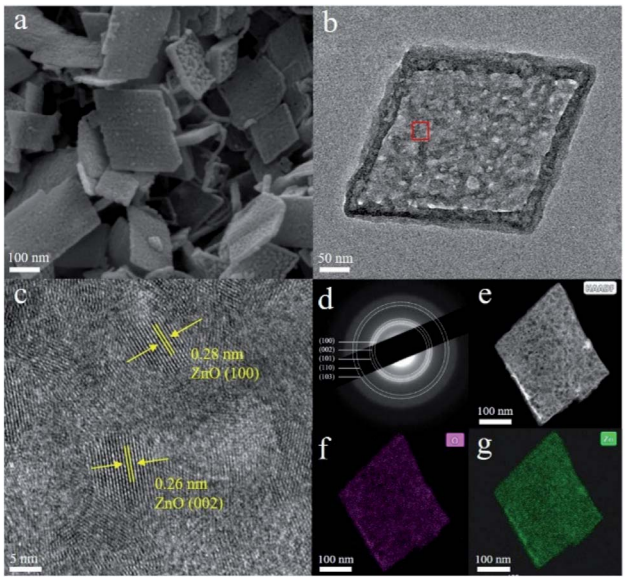

Fig. 2 (a and b) TEM images of porous d-ZnO NSs. (c) The HRTEM image recorded on the framed area in (b). (d) The corresponding SAED pattern. (e) HAADF-STEM image and (f and g) corresponding elemental maps of O and Zn of the porous d-ZnO NSs.

and the electrostatic adsorption effect.[6,16,22] The pore size distribution of d-ZnO NSs is relatively uniform, and the length scale of the pores ranges from 2 to 8 nm with an average value at 4 nm (Fig. S5b†), which is beneficial for providing high and uniform SERS activity. The SERS spectra of 4-mercaptopyridine (4MPY) and 4-aminothiophenol (4ATP) molecules adsorbed on d-ZnO NSs are obtained under different laser illuminations as shown in Fig. S6.† The results demonstrate that the SERS intensities of the 4MPY molecule (1119 cm^{-1}: C–S stretching modes, 1324 cm^{-1}: C–H stretching vibration modes, 1595 cm^{-1}: C=C phenyl ring vibration modes)[35] and 4ATP molecule (1095 cm^{-1}: C–S stretching vibration modes, 1149 cm^{-1}: C–H stretching vibration modes, 1392 and 1440 cm^{-1}: δ(C–H) + δ(C–C) stretching vibration modes, 1588 cm^{-1}: C=C stretching mode of the benzene ring)[36] excited with a 532 nm laser are clearly stronger than those at 633 and 785 nm. The appreciable SERS vibration peak shifts of probe molecules adsorbed on d-ZnO NSs compared to the normal Raman peak are derived from stronger semiconductor–molecule interactions.[6,23] Charge transfer resonance, chemical bonding, and the electron level vibration coupling effect that occur in semiconductor–molecule SERS systems can significantly change the electromagnetic environment of the probe molecule, which leads to an obvious peak shift of the molecular Raman vibration modes. Motivated by the PL emission spectrum (Fig. S7†), the result clearly shows that the band gap emission of ZnO NSs is ~375 nm (3.31 eV). The obvious PL peak induced by surface defects is at ~600 nm (2.07 eV), thus the energy level position of surface defect states is ~2.07 eV higher than that of the VB edge. Therefore, it is obvious that a more facile and efficient PICT process promoted by surface defect states can be obtained in a d-ZnO NS–molecule system illuminated by a 532 nm laser (2.33 eV), rather than

633 nm (1.96 eV) and 785 nm (1.58 eV), resulting in the increase of molecular polarizability.[37] The SPR position of d-ZnO NSs is not in the 400–800 nm light region, which is confirmed from the UV-Vis absorption spectrum (Fig. S8†), ruling out the SPR effect in the ZnO NS SERS substrate. Note that the effect of intrinsic molecular resonance is ruled out, as 4MPY and 4ATP molecules are non-resonant in the visible light region (Fig. S9†). New Raman peaks of the 4MPY molecule appear at 1020, 1245, 1324, and 1595 cm^{-1} and new vibration peaks of the 4ATP molecule at 990, 1392, and 1440 cm^{-1} are categorized as non-totally symmetric modes (b_2 modes).[23] According to the Herzberg–Teller rule, the selectively enhanced b_2 modes in d-ZnO NSs are derived from the charge transfer mechanism,[38,39] and the feature of selective enhancement of d-ZnO NSs is a unique advantage for identifying targeted molecules in a complex system. The limit of detection values for 4MPY, Crystal Violet (CV), and Rhodamine 6G (R6G) molecules adsorbed on d-ZnO NSs are 1×10^{-6} M, 2×10^{-7} M, and 1×10^{-7} M, respectively, indicating the good SERS activity of d-ZnO NSs at room temperature (Fig. S10†).

As the number of photo-induced electrons participating in the PICT process can be severely decreased by phonon-assisted non-radiative recombination,[27] weakening of lattice thermal vibration under low-temperature conditions could effectively reduce the phonon-assisted relaxation and provide efficient PICT transitions within the substrate–molecule system. For steady-state conditions, the number of electrons ($N(T)$) at defect states is determined using eqn (1), as a function of temperature T:[40–42]

$$N(T) = \frac{N_0}{1 + (\tau/\tau_0)e^{-E_{defect}/kT}} \quad (1)$$

In the expression, k is the Boltzmann constant, τ is the exciton lifetime exceeding 100 ps, and N_0 is the number of electrons when the temperature is 0 K. τ_0 is regarded as the effective scattering time. E_{defect} represents the activation energy, which describes the energy of defect states. For a semiconductor substrate, SERS enhancement (I_{Raman}) is determined by the Raman scattering cross section (σ^R_{ads}) of the adsorbed molecule: $I_{Raman} \propto \sigma^R_{ads}$. According to eqn (1), the number of electrons on surface defect states is determined by the surface defect energy level (E_{defect}) and temperature (T). The number of photo-induced electrons at defect states can be largely increased with the decreased temperature due to the low temperature-reduced phonon-assisted non-radiative recombination. This effect will significantly promote PICT transition possibility from the semiconductor to probe molecule and increase the molecular Raman scattering cross section (σ^R_{ads}),[25,43] as exhibited in eqn (2). Thus, low temperature will play a significant role in facilitating an efficient charge transfer process, magnifying the Raman scattering cross-section (σ^R_{ads}), and enabling remarkable SERS enhancement (I_{Raman}), according to eqn (3).

$$\sigma^R_{ads} \propto \frac{N_0}{1 + (\tau/\tau_0)e^{-E_A/kT}} \propto N_0 e^{E_A/kT} \quad (2)$$

$$I_{Raman} \propto 1/T \quad (3)$$

Accordingly, the favorable PICT efficiency of the d-ZnO NSs–molecule surface complex can be boosted by the suppressed phonon-assisted relaxation at a low temperature, which is beneficial to obtain a remarkable SERS EF. To verify this, we carefully performed PL emission spectroscopy, which is a useful tool for measuring the band gap, surface defect energy level, photo-induced electron concentration, and impurity element of semiconductor materials.[44] The PL emission spectra of d-ZnO NSs are obtained under different temperature conditions *in situ* (Fig. 3a), and the oxygen vacancy defect-induced PL peak (~600 nm)[22] intensity is dramatically enhanced with the decrease of temperature. The PL emission peak intensity of oxygen vacancy defect states at a low temperature (77 K) is obviously increased by ~3 fold compared to the intensity at room temperature (293 K). This clearly indicates that the number of photo-induced electrons on the surface defect energy level is greatly increased due to the effectively suppressed phonon-assisted non-radiative recombination and the reduced carrier traps at a low temperature. The decrease of trapped photo-induced electrons at surface defect states will facilitate the charge transfer process from d-ZnO NSs to molecules under laser illumination, suggesting an effective strategy for promoting PICT transitions and magnifying the molecular Raman scattering cross-section.

To explore the mechanism of the low temperature-assisted and highly efficient PICT process between the d-ZnO NSs and probe molecule, the temperature-dependent SERS experiment was carefully performed *in situ*. The results demonstrate that the Raman vibration peak intensities of the R6G molecule gradually increase with decreasing temperature from 293 K to

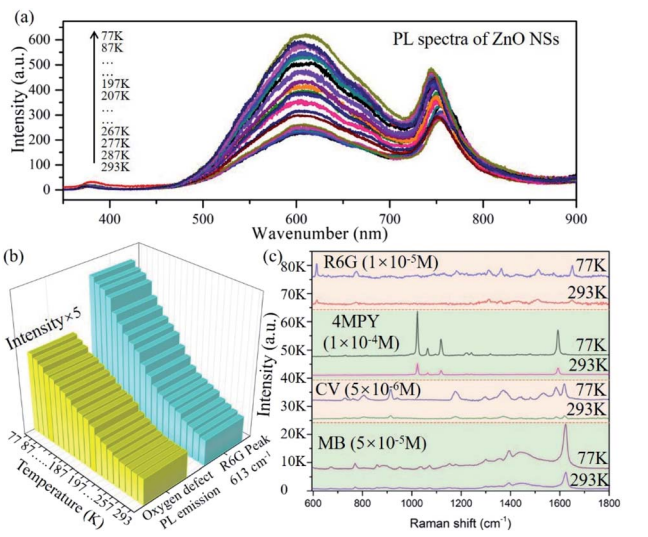

Fig. 3 (a) PL emission spectra of porous d-ZnO NSs acquired at different temperatures. Laser wavelength: 325 nm; laser power: 1 mW; lens: 40× near ultraviolet objective; acquisition time: 2 s. (b) Oxygen vacancy defect-induced PL peak (~600 nm) emission intensity of porous d-ZnO NSs, and the SERS peak (613 cm^{-1}) of the R6G molecule on d-ZnO NSs at different temperatures. (c) SERS spectra of R6G, 4MPY, CV, and MB molecules adsorbed on d-ZnO NSs at temperatures of 77 K and 293 K, respectively. Laser wavelength: 532 nm; laser power: 0.5 mW; lens: 50× objective; acquisition time: 2 s.

77 K, as shown in Fig. S11.† The C–H out-of-plane bending vibration peak intensity (613 cm^{-1}; b_2 mode)[45] of the R6G molecule adsorbed on d-ZnO NSs at different temperatures is shown in Fig. 3b. The Raman vibration mode intensity is enhanced ~4 times at a low temperature compared to that at room temperature, which is consistent with the strongly enhanced oxygen vacancy PL emission peak at a low temperature (Fig. 3b). SERS spectra comparison of the 4MPY molecule (1×10^{-4} M) on d-ZnO NSs at room temperature (293 K) and a low temperature (77 K) is shown in Fig. 3c, in which the Raman vibration signal is obviously boosted. The b_2 vibration modes (1072 and 1123 cm^{-1}) exhibit the largest EF in the d-ZnO NS–4MPY system, illustrating that the PICT vibrational coupling has been significantly promoted at low temperature. For the case of dye molecules adsorbed on d-ZnO NSs, CV and methylene blue (MB) molecules also exhibit a higher SERS intensity at a low temperature (77 K) than room temperature (Fig. 3c), indicating that the low-temperature SERS strategy possesses good universality for magnifying the Raman signal of various target molecules. The Raman vibration modes of the CV and MB molecules[46,47] are discussed in the ESI.†

It is clear that d-ZnO NSs exhibit remarkable SERS sensitivity with a 1×10^{-7} M limit of detection for the 4MPY molecule at low temperature (77 K), as shown in Fig. 4a. The Raman intensity of the probe molecules could be amplified by low temperature without the ZnO substrate (Fig. S12†), and the enhancement factor (EF) of 4MPY molecules is 1.47. The corresponding EF value for the 4MPY molecule absorbed on d-ZnO NSs at low temperature is estimated to be 7.7×10^5 according to the SERS peak intensity at 1605 cm^{-1} (details of EF calculations are discussed in the ESI, Fig. S13a†). The supersaturation adsorption effect resulting in a falsely high EF has been ruled out by choosing the 4MPY molecule solution concentration below 1×10^{-3} M, and the relationship between the 4MPY concentration and corresponding SERS peak intensity is shown in Fig. S13b.† Fig. 4b illustrates the facilitated PICT transition pathways from the d-ZnO NSs to 4MPY molecules, which should be attributed to the low temperature-increased photo-induced electrons in d-ZnO NSs. The highest occupied molecular orbital (HOMO) and lowest unoccupied molecular orbital (LUMO) energy level positions of the 4MPY molecule are located at 6.32 and 2.95 eV below the vacuum level, respectively.[16] The PICT transition efficiency from d-ZnO NSs (|C⟩ or |S⟩ states) to the LUMO of 4MPY (|K⟩ state) can be significantly promoted by the increased photo-induced electrons on the oxygen defect energy level, owing to the suppressed phonon-assisted non-radiative recombination at low temperature. Low temperature-boosted PICT transitions within the substrate–molecule system can effectively amplify molecular polarizability and enhance the Raman intensity. During the measurements from the normal temperature to low temperature, the crystal phase change possibility of d-ZnO NSs is excluded by the Raman spectrum, as shown in Fig. S14.† The Raman spectrum result demonstrates d-ZnO NSs maintaining the wurtzite phase[48] at a low temperature (77 K), and the Raman vibration modes of d-ZnO NSs do not have any peak shift compared to that at room

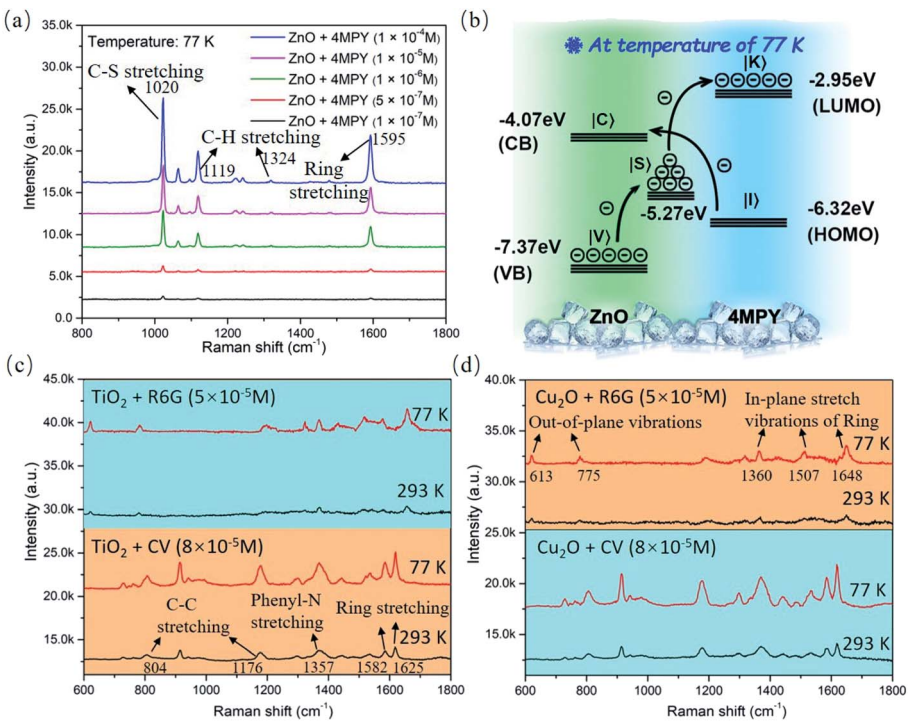

Fig. 4 (a) SERS spectra of the 4MPY molecule adsorbed on porous d-ZnO NSs with different concentrations measured at temperature of 77 K. (b) PICT process between d-ZnO NSs and the 4MPY molecule is facilitated at a low temperature; 532 nm laser illumination. SERS intensity comparison of the R6G and CV molecules adsorbed on d-TiO_2 (c) and d-Cu_2O (d) NPs at temperature of 77 K and 293 K. Laser power: 0.5 mW; lens: 50× objective; acquisition time: 2 s.

temperature. In addition, Fig. S15† shows the excellent spectral uniformity and repeatability of d-ZnO NSs.

Significantly, we further demonstrate that this low temperature-assisted high-efficiency PICT strategy can be applicable to general semiconductor nanomaterials, such as d-TiO_2 and d-Cu_2O nanomaterials. The characterization data (TEM images and XRD patterns) of d-TiO_2 and d-Cu_2O NPs are shown in Fig. S16,† which are synthesized by a chemical precipitation method[49] (the synthesis process is given in the ESI†). Fig. S17† demonstrates that the surface defect-induced PL emission peak (~680 nm) intensities of d-TiO_2 and d-Cu_2O NPs are obviously enhanced as the temperature decreases, indicating more photo-induced electrons on the defect energy level due to the suppressed phonon-assisted relaxation at low temperature. Control temperature-dependent SERS measurements of four d-TiO_2@R6G, d-TiO_2@CV, d-Cu_2O@R6G, and d-Cu_2O@CV surface complexes are performed at low and room temperatures, respectively, as shown in Fig. 4a and b. The SERS signals of the R6G and CV molecules on d-TiO_2, and d-Cu_2O substrates are undoubtedly boosted at a low temperature (77 K), which are ascribed to the increased number of photo-induced electrons participating in the PICT process. These results further confirm that the charge transfer efficiency from d-TiO_2 (d-Cu_2O) NPs to probe molecules is explicitly facilitated at low temperature. Based on the obviously enhanced SERS activity of d-ZnO, d-TiO_2, and d-Cu_2O NPs, the low temperature-SERS strategy is established to be a facile approach to achieve a high PICT efficiency in semiconductor–molecule systems. The above analysis clearly demonstrates that the universality of the proposed low-temperature SERS strategy can be applicable to other types of semiconductors.

Conclusions

Porous d-ZnO NSs with abundant surface defects have been successfully synthesized as an ideal sample to illustrate a highly efficient PICT process from the substrate to molecule at a low temperature. The facilitated PICT process is dominated by the increased number of photo-induced electrons due to the significant reduction of phonon-assisted non-radiative recombination at low temperature. The increased number of photo-induced electrons on the surface defect states of d-ZnO NSs is verified through low-temperature PL emission spectroscopy, and the temperature-dependent SERS activity of d-ZnO NSs is measured *in situ*. The PL intensity of the oxygen vacancy is obviously enhanced due to the suppressed phonon-assisted relaxation and carrier traps at a low temperature, and the decrease of trapped photo-induced electrons at surface defect states effectively facilitates PICT within the d-ZnO–molecule system. Plentiful surface defect states and the low temperature synergistically endow porous d-ZnO NSs with remarkable SERS activity and an EF of 7.7×10^5. The results of this study establish that the new low temperature-based strategy could facilitate the PICT transitions and boost semiconductor SERS activity. Interestingly, the proposed strategy is also applicable to other semiconductor nanomaterials, such as d-TiO_2 and d-Cu_2O NPs, demonstrating the excellent expandability and universality of this facile approach. Finally, the low temperature-boosted high-efficiency PICT strategy not only provides an important insight into the chemical mechanism but also guides further developments for exploring high SERS-active semiconductor substrates.

Conflicts of interest

The authors declare no competing financial interest.

Acknowledgements

This work was financially supported by the funding support from the STS project from the Chinese Academy of Sciences (KFJ-STS-ZDTP-061), National Natural Science Foundation of China (31971292, U1432114, 51532001, 21875008, and 51801007), China Postdoctoral Science Foundation (2019T120534, and 2018M640576), Zhejiang Province Key Research Project (2019C03058), Strategic Priority Research Program of Chinese Academy of Sciences (XDB36000000), Zhejiang Province Financial Supporting (LQ20E020003), and Natural Science Foundation of Ningbo (2019A610024 and 2018A610218).

Notes and references

1 J. F. Li, Y. F. Huang, Y. Ding, Z. L. Yang, S. B. Li, X. S. Zhou, F. R. Fan, W. Zhang, Z. Y. Zhou, D. Y. Wu, B. Ren, Z. L. Wang and Z. Q. Tian, *Nature*, 2010, **464**(7287), 392–395.
2 Y. Fang, N. H. Seong and D. D. Dlott, *Science*, 2008, **321**(5887), 388–392.
3 E. J. Blackie, E. C. L. Ru and P. G. Etchegoin, *J. Am. Chem. Soc.*, 2009, **131**(40), 14466–14472.
4 K. Liu, Y. C. Bai, L. Zhang, Z. B. Yang, Q. K. Fan, H. Q. Zheng, Y. D. Yin and C. B. Gao, *Nano Lett.*, 2016, **16**(6), 3675–3681.
5 S. M. Feng, M. C. D. Santos, B. R. Carvalho, R. Lv, Q. Li, K. Fujisawa, A. L. Elías, L. Yu, N. Perea-lópez, M. Endo, M. Pan, M. A. Pimenta and M. Terrones, *Sci. Adv.*, 2016, **2**(7), e1600322.
6 I. Alessandri and J. R. Lombardi, *Chem. Rev.*, 2016, **116**(24), 14921–14981.
7 D. L. Jeanmaire and R. P. Vanduyne, *J. Electroanal. Chem.*, 1977, **84**, 1–20.
8 M. G. Albrecht and J. A. Creighton, *J. Am. Chem. Soc.*, 1977, **99**(15), 5215–5217.
9 S. Nie and S. R. Emory, *Science*, 1997, **275**(5303), 1102–1106.
10 J. F. Li, Y. J. Zhang, S. Y. Ding, R. Panneerselvam and Z. Q. Tian, *Chem. Rev.*, 2017, **117**(7), 5002–5069.
11 Z. Zheng, S. Cong, W. Gong, J. Xuan, G. Li, W. Lu, F. Geng and Z. Zhao, *Nat. Commun.*, 2017, **8**, 1993.
12 X. T. Wang, W. S. Shi, G. W. She and L. X. Mu, *J. Am. Chem. Soc.*, 2011, **133**(41), 16518–16523.
13 L. Yang, Y. Peng, Y. Yang, J. Liu, H. Huang, B. Yu, J. Zhao, Y. Lu, Z. Huang, Z. Li and J. R. Lombardi, *Adv. Sci.*, 2019, **6**(12), 1900310.
14 Q. Zhang, X. Li, Q. Ma, Q. Zhang, H. Bai, W. Yi, J. Liu, J. Han and G. Xi, *Nat. Commun.*, 2017, **8**, 14903.

15 J. Lin, W. Ren, A. Li, C. Yao, T. Chen, X. Ma, X. Wang and A. Wu, *ACS Appl. Mater. Interfaces*, 2020, **12**(4), 4204–4211.
16 W. Ji, L. Li, W. Song, X. Wang, B. Zhao and Y. Ozaki, *Angew. Chem., Int. Ed.*, 2019, **58**, 1–6.
17 J. Lin, W. Hao, Y. Shang, X. Wang, D. Qiu, G. Ma, C. Chen, S. Li and L. Guo, *Small*, 2018, **14**(8), 1703274.
18 X. X. Xue, W. D. Ruan, L. B. Yang, W. Ji, Y. F. Xie, L. Chen, W. Song, B. Zhao and J. R. Lombardi, *J. Raman Spectrosc.*, 2012, **43**(1), 61–64.
19 I. Alessandri, *J. Am. Chem. Soc.*, 2013, **135**(15), 5541–5544.
20 D. Y. Qi, L. Lu, L. Z. Wang and J. L. Zhang, *J. Am. Chem. Soc.*, 2014, **136**(28), 9886–9889.
21 S. Cong, Y. Y. Yuan, Z. G. Chen, J. Y. Hou, M. Yang, Y. L. Su, Y. Y. Zhang, L. Li, Q. W. Li, F. X. Geng and Z. G. Zhao, *Nat. Commun.*, 2015, **6**, 7800.
22 J. Lin, Y. Shang, X. X. Li, J. Yu, X. T. Wang and L. Guo, *Adv. Mater.*, 2017, **29**(5), 1604797.
23 X. T. Wang, W. X. Shi, Z. Jin, W. F. Huang, J. Lin, G. S. Ma, S. Z. Li and L. Guo, *Angew. Chem., Int. Ed.*, 2017, **129**(33), 9983–9987.
24 A. Li, J. Lin, Z. Huang, X. Wang and L. Guo, *iScience*, 2018, **10**, 1–10.
25 X. Wang, W. Shi, S. Wang, H. Zhao, J. Lin, Z. Yang, M. Chen and L. Guo, *J. Am. Chem. Soc.*, 2019, **141**, 5856–5862.
26 Z. J. Yong, S. Q. Guo, J. P. Ma, J. Y. Zhang, Z. Y. Li, Y. M. Chen, B. B. Zhang, Y. Zhou, J. Shu, J. L. Gu, L. R. Zheng, O. M. Bakr and H. T. Sun, *J. Am. Chem. Soc.*, 2018, **140**(31), 9942–9951.
27 P. Tamarat, M. I. Bodnarchuk, J. Trebbia, R. Erni, M. V. Kovalenko, J. Even and B. Lounis, *Nat. Mater.*, 2019, **18**(7), 717–724.
28 R. Milot, M. Klug, C. Davies, Z. Wang, H. Kraus, H. Snaith, M. Johnston and L. Herz, *Adv. Mater.*, 2018, **30**, 1804506.
29 A. A. Lohar, A. Shinde, R. Gahlaut, A. Sagdeo and S. Mahamuni, *J. Phys. Chem. C*, 2018, **122**(43), 25014–25020.
30 J. R. Lombardi, R. L. Birke, T. H. Lu and J. Xu, *J. Chem. Phys.*, 1986, **84**(8), 4174–4180.
31 M. Osawa, N. Matsuda, K. Yoshii and I. Uchida, *J. Phys. Chem.*, 1994, **98**(48), 12702–12707.
32 Y. F. Wang, W. D. Ruan, J. H. Zhang, B. Yang, W. Q. Xu, B. Zhao and J. R. Lombardi, *J. Raman Spectrosc.*, 2009, **40**(8), 1072–1077.
33 D. Glass, E. Cortés, S. Ben-Jaber, T. Brick, C. S. Blackman, C. R. Howle, R. Quesada-Cabrera, I. P. Parkin and S. A. Maier, *Adv. Sci.*, 2019, **6**(22), 1901841.
34 Q. Liu, L. Jiang and L. Guo, *Small*, 2014, **10**(1), 48–51.
35 L. Jiang, T. T. You, P. G. Yin, Y. Shang, D. F. Zhang, L. Guo and S. H. Yang, *Nanoscale*, 2013, **5**(7), 2784–2789.
36 M. T. Sun and H. X. Xu, *ChemPhysChem*, 2009, **10**(2), 392–399.
37 Y. Yin, P. Miao, Y. M. Zhang, J. C. Han, X. H. Zhang, Y. Gong, L. Gu, C. Y. Xu, T. Yao and P. Xu, *Adv. Funct. Mater.*, 2017, **27**(16), 1606694.
38 J. R. Lombardi and R. L. Birke, *J. Phys. Chem. C*, 2014, **118**(20), 11120–11130.
39 N. Bontempi, l. Carletti, C. D. Angelis and I. Alessandri, *Nanoscale*, 2016, **8**(6), 3226–3231.
40 Z. T. Wu, Z. Z. Luo, Y. T. Shen, W. W. Zhao, W. H. Wang, H. Y. Nan, X. T. Guo, L. T. Sun, X. R. Wang, Y. M. You and Z. H. Ni, *Nano Res.*, 2016, **9**(12), 3622–3631.
41 G. Bacher, H. Schweizer, J. Kováč, A. Forchel, H. Nickel, W. Schlapp and R. Lösch, *Phys. Rev. B: Condens. Matter Mater. Phys.*, 1991, **43**(11), 9312–9315.
42 Y. M. You, X. X. Zhang, T. C. Berkelbach, M. S. Hybertsen, D. R. Reichman and T. F. Heinz, *Nat. Phys.*, 2015, **11**(6), 477–481.
43 X. T. Wang and L. Guo, *Angew. Chem., Int. Ed.*, 2020, **59**(11), 4231–4239.
44 S. Baek, Y. C. Kim and J. M. Myoung, *Appl. Surf. Sci.*, 2019, **480**, 122–130.
45 F. Q. Huang, G. S. Ma, J. Z. Liu, J. Lin, X. T. Wang and L. Guo, *Small*, 2016, **12**(39), 5442–5448.
46 M. V. Cañamares, C. Chenal, R. L. Birke and J. R. Lombardi, *J. Phys. Chem. C*, 2008, **112**(51), 20295–20300.
47 S. D. Roy, M. Ghosh and J. Chowdhury, *J. Raman Spectrosc.*, 2015, **46**(5), 451–461.
48 H. Y. Shi, B. Deng, S. L. Zhong, L. Wang and A. W. Xu, *J. Mater. Chem.*, 2011, **21**(33), 12309–12315.
49 D. F. Zhang, H. Zhang, L. Guo, K. Zheng, X. D. Han and Z. Zhang, *J. Mater. Chem.*, 2009, **19**(29), 5220–5225.

